AMC-backed Twin Arrow Antenna for Wearable Electronic Travel Aid System at 24 GHz

A. Flórez Berdasco *Graduate Student Member, IEEE*, M. E. de Cos Gómez *Member, IEEE*, J. Laviada, F. Las-Heras *Senior Member, IEEE*

***Abstract*—An ultra-compact wearable antenna, for electronic travel aid (ETA) applications in the 24.05-24.25 GHz frequency band, is presented. The artificial magnetic conductor (AMC)-antenna combination reduces the backward radiation to the wearing person, while improves antenna's radiation properties and bandwidth without increasing its area. Prototypes of the AMC-antenna have been fabricated and measured. In order to test its performance for the application, imaging has been conducted by means of synthetic aperture radar (SAR) techniques by placing the antenna in the arm of a user to take advantage of natural body movement. Electromagnetic images have been obtained and the target has been identified, demonstrating the suitability of the AMC-antenna for the ETA system.**

***Index Terms*—Antenna with metasurface, AMC, mmWave radar, imaging, mmWave antenna, ETA.**

I. Introduction

MORE than 2 billion people worldwide suffer from vision problems that, in the worst cases, limit their daily life [1]. The white cane is the most widespread mobility aid, along with guide dogs. However, they are not enough for full autonomy, as the former does not detect obstacles at torso height and the latter needs strong training [2]. Thus, numerous electronic travel aid systems (ETA) have been developed in the last years. Most of them are based on ultrasound sensors and video cameras [2]–[4], although there are alternatives that use technologies such as near-field communication (NFC), infrared sensors, and others [5].

Radar technology stands out as one of the most promising technologies for ETAs, especially at mmWave frequencies, where compact devices suitable for portable applications are available. Moreover, it works in all weather and visibility conditions and detects both, visible and hidden objects. In addition, radars can be worn under clothing, as the electromagnetic wave signals that they emit, can easily penetrate through fabrics, making their use completely unobtrusive. Therefore, due to all the advantages of radar technology, it seems entirely appropriate as an alternative to the aforementioned systems.

The angular resolution of the system is limited by the radar aperture [6], so synthetic aperture radar (SAR) techniques are going to be implemented. This solution has been widely deployed for a large number of applications in recent years such as nondestructive testing, medical imaging or security [7]–[9]. SAR is based on moving the antenna and taking measurements at a set of positions to coherently add all the reflected signals, in order to obtain high resolution images. In this case, they are implemented by taking advantage of the natural movement of the user [10], due to the wearable nature of the application.

Portable and wearable systems require small and compact antennas, that can be easily carried by the user. Miniaturized, lightweight and low-profile planar antennas are preferred for their comfort and convenience for wearable applications. From the radar application point of view, it is necessary to point out some considerations. Antennas with narrow-beam radiation patterns, which enhance directivity, are favored for long distance applications, so that a larger range of operation is obtained. However, if near-field SAR techniques are going to be explored, wide-beam radiation patterns seem better as the complete scene can be illuminated at all the positions along the aperture. Therefore, a trade-off solution between range and area of coverage must be found. Moreover, our recent work evaluating the performance of different antennas for ETA application illustrates how, for short distance detection, antennas with low directivity exhibit better performance than high gain antennas, which can provide anomalous results along their electrically larger dimension [11].

In this work, an AMC-backed twin Arrow Antenna designed, operative in the 24.05-24.25 GHz frequency band, for a wearable ETA system is shown. In order to test its suitability for the target application, SAR measurements taking advantage of the natural movement of the user have been performed in the near-field of the aperture and electromagnetic images have been obtained to detect targets.

The paper is organized as follows: first, the design procedure of the antenna and the AMC are exposed. Later, the combination of both structures is shown, and the results are compared with the original antenna. Then, the fabrication methodology is explained, and the measurement outcomes are confronted with the simulated ones. After that, the AMC-antenna performance in the real radar application is shown and imaging results are displayed and analyzed. Finally, conclusions are drawn.

II. Antenna design

A novel twin arrow antenna, that operates in the 24.05 to 24.25 GHz frequency band, is presented. It follows the

Manuscript received April 19, 2024; revised August 16, 2021.

This work was supported in part by the Ministerio de Ciencia e Innovación of Spain under the Formación Personal Investigador (FPI) Grant MCIU-20-PRE2019-089912 and under Project META-IMAGER PID2021-122697OB-I00 and in part by the Gobierno del Principado de Asturias under Project AYUD-2021-51706.

Alicia Flórez Berdasco, María Elena de Cos Gómez, Jaime Laviada and Fernando Las-Heras are with the Department of Electrical Engineering, University of Oviedo, Spain. (e-mail: florezalicia@uniovi.es, medecos@uniovi.es; laviadajaime@uniovi.es; flasheras@uniovi.es).

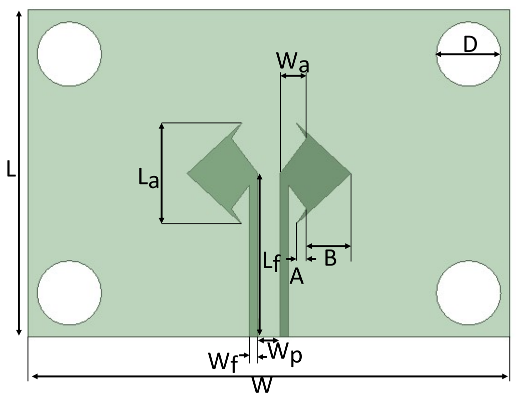

Fig. 1: Antenna geometry

TABLE I: Antenna dimension (mm)

L	W	L_f	W_f	W_p	L_a	W_a	A	B	D	h
9.6	14.1	4.8	0.25	0.45	0.87	2.96	0.3	1.6	1.9	0.762

operating principles of a planar dipole antenna, however, the shape of the radiating elements has been modified to enhance its performance. RO3003 ($\varepsilon_r = 3.0$, $\tan\delta = 0.0013$ and $h = 0.762$ mm) has been selected as dielectric substrate since its intermediate value of relative dielectric permitivity allows obtaining proper antenna size for fabrication suitability. The two radiating elements and their narrow feeding lines are metallic and have been optimized using the electromagnetic software simulator HFSS. Fig. 1 shows the antenna geometry, and the final dimensions are summarized in Table I.

The antenna exhibits proper impedance matching from 23.2 to 24.8 GHz. It provides 4.13 dBi of gain (G) and 4.26 dB of directivity (D) at 24.15 GHz. Therefore, the radiation efficiency (η) is 97 %. As the antenna is not backed with a ground plane, it shows a very low front-to-back ratio (FTBR) of 0.25 dB. All the radiation parameters of the antenna are collected in Table II.

A. Artificial Magnetic Conductor Design

With the aim of reducing the backward radiation, an AMC metasurface has been designed to back the antenna. Common metallic ground planes (electric conductors) must be placed at a distance of at least one quarter wavelength from the antenna. If this minimum distance is not observed, there are no constructive interferences, and the antenna is shorted. AMC is a type of metasurface that has the ability to reflect the incident electromagnetic field in phase in the bandwidth that comprises the frequencies for which the phase of the reflection coefficient is between ±90º [12]. This characteristic allows placing the AMC closer or even attached to the antenna [13]–[17].

A squared metallization has been situated over a grounded dielectric (RO3003) to create the AMC unit-cell. A simple geometry has been selected to facilitate its fabrication. The geometry of the unit-cell is shown in Fig. 2 with its reflection coefficient. Floquet port and periodic boundary conditions were considered in simulation for the unit-cell optimization based on the phase of the reflection coefficient. The resulting dimensions of the unit-cell are $P = 3.2$ mm, $g = 0.5$ mm

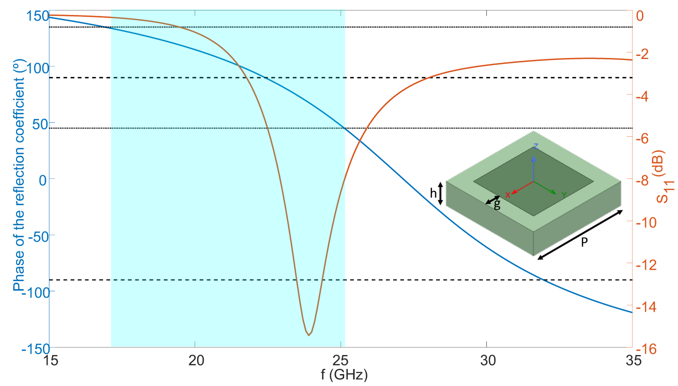

Fig. 2: Simulated antenna reflection coefficient and AMC reflection phase and its geometry. Light blue strip shows the working band of the AMC.

and $h = 0.762$ mm. The resonance frequency of the AMC is 26.6 GHz and the AMC operating bandwidth is 22-31.1 GHz (see Fig. 2).

B. AMC-antenna Combination

The AMC metasurface has been arranged under the antenna, so that the backward radiation to the wearing person will be reduced. The $90º \pm 45º$ reflection phase region of the AMC, is the optimum operating bandwidth when the metasurface is combined with a dipole antenna [18]. Fig. 2 shows the antenna reflection coefficient with the AMC reflection phase. It can be observed that the resonance frequency of the antenna is included in the frequency band in which the reflection phase of the AMC is between $90º \pm 45º$, which has been highlighted in light blue.

The AMC has been placed under the antenna without any gap between them. It should be noted that the unit-cell under the feed lines has been removed so as not to disturb the feeding network. The final geometry of the combined structure is presented in Fig. 3, with the reflection coefficient of both, the antenna alone and the AMC-antenna. The AMC-antenna shows a much wider bandwidth than the antenna without metasurface, however, both operate in the target frequency band. The radiation pattern cuts are depicted in Fig. 4. It can be observed that the AMC metasurface reduces the backward radiation and slightly modifies the radiation pattern, so that a more directive one is observed. Table II collects the main radiation properties of both antennas. It can be concluded that the AMC-antenna improves around 2 dB both, directivity and gain with respect to the original antenna. The radiation efficiency keeps high across the whole bandwidth. The great advantage of placing an AMC metasurface behind the antenna is raising the FTBR parameter by approximately 15 dB, so that, when the AMC is placed under the antenna, the backward radiation to the body is significantly reduce, which is essential in wearable devices. Therefore, all the radiation properties and the bandwidth of the original antenna have been improved while preserving the initial area. The unavoidable thickness increase (only due to the AMC as there is no layer between it and the antenna) however has no impact on the resulting

This article has been accepted for publication in IEEE Antennas and Wireless Propagation Letters. This is the author's version which has not been fully edited and content may change prior to final publication. Citation information: DOI 10.1109/LAWP.2024.3378012

TABLE II: Radiation properties for the antenna and AMC-antenna.

	BW(%)	F (GHz)	G (dBi)	D (dB)	η (%)	FTBR (dB)
Antenna	6.21	24.05	4.14	4.26	97.3	0.25
		24.15	4.13	4.26	97.1	0.25
		24.25	4.01	4.26	94.4	0.25
AMC-antenna	15.7	24.05	6.72	6.72	100	14.32
		24.15	6.73	6.74	99.8	15.58
		24.25	6.74	6.77	99.3	16.12

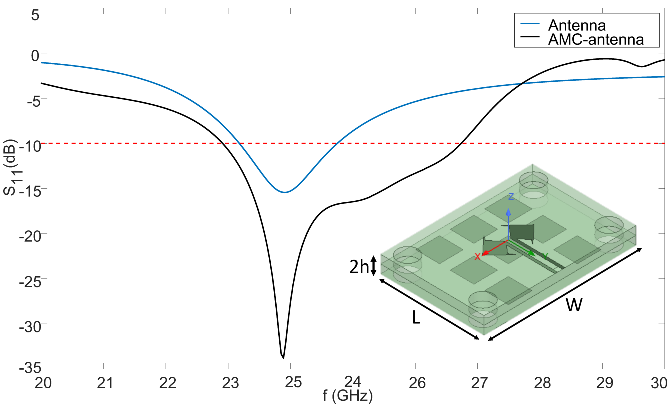

Fig. 3: S_{11} comparison for the antenna and the AMC-antenna.

antenna comfort and wearability. Hence, an ultra-compact and operative antenna has been achieved to be used in ETA applications.

C. Fabrication and Measurement

Prototypes of the AMC-antenna have been fabricated using laser micromachining. Each element (antenna and AMC) is manufactured separately and then, they have been fixed using nylon screws, as it can be appreciated in Fig. 5. It depicts measured and simulated reflection coefficient results of the AMC-antenna. The measured trace has been slightly shifted downwards in frequency; however, it shows proper impedance matching in the frequency bandwidth of interest. Discrepancies between simulated and measured results can be attributed to several issues. On the one hand, manufacturing tolerances can cause the displacement of the resonance frequency. On the other hand, the connector is soldered by hand to the narrow strips and its size is very large compared to the antenna, which

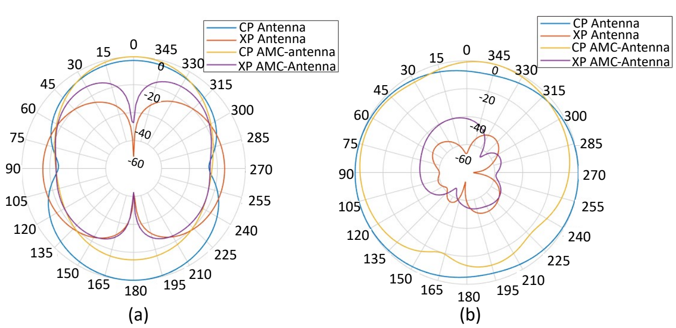

Fig. 4: Radiation pattern cuts. (a) Phi=0º, (b) Phi=90º.

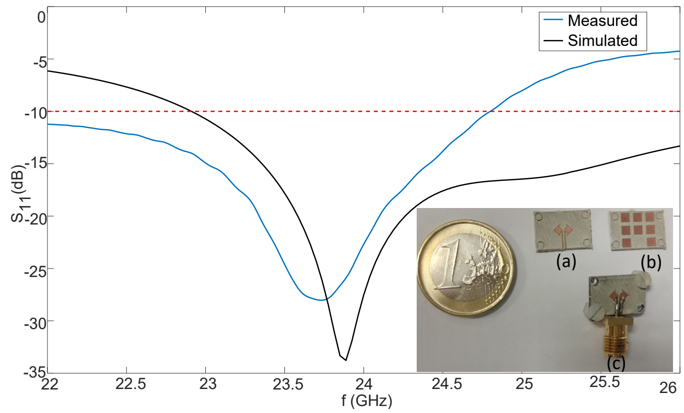

Fig. 5: Comparison between the measured and simulated S_{11} of the AMC-antenna together with the antennas prototype. (a) Antenna prototype, (b) AMC prototype, (c) AMC-antenna prototype.

can produce these mismatches. In addition, the antenna and the AMC are aligned through the screws, but it is possible that small misalignment may occur, which can result in frequency shifts. Nevertheless, the measured trace has deviated by just 0.84% from the simulated one.

D. Comparison with Other Millimeter-Wave Antennas at 24 GHz

A brief comparison with the state-of-the-art antennas at 24 GHz is provided to endorse the achievements of this work. Despite using dielectric with practically the same ε_r, the AMC-antenna outperforms [19], [20] in area and bandwidth. It also overcomes [19] in gain. Although it provides slightly lower gain than [20], the AMC-antenna triples its radiation efficiency. Moreover, [20] is fabricated in paper, which is not the best material for a portable systems, as it can be easily damaged. Compared to those on substrates with slightly higher ε_r, the AMC-antenna overcomes [21], [22] in bandwidth and gain, with a more compact design in area. In addition, it exhibits better FTBR than [22]. [23] presents a bigger antenna in comparison with the one of this paper, even though a material with a higher ε_r is used. Besides, it provides half the bandwidth, despite requiring a greater thickness of material. It shows better gain, however, η and FTBR are not given.

TABLE III: State-of-the-art antennas at 24 GHz.

	Size (mm^3)	ε_r	BW (%)	G (dBi)	η (%)	FTBR (dB)
[19]	$76 \times 76 \times 0.13$	3	3.8	4.8	-	-
[20]	$20 \times 25 \times 0.23$	2.9	2.3	7.4	35	-
[21]	$36.5 \times 53 \times 0.1$	3.35	0.8	5.81	-	-
[22]	$23 \times 15 \times 0.254$	3.48	6.6	4.24	-	9.23
[23]	$24 \times 24 \times 1.6$	6.4	8	9	-	-
AMC-antenna	$9.6 \times 14.1 \times 1.524$	3	15.7	6.73	99.8	15.58

III. Imaging Testing

Antenna performance is evaluated experimentally for the intended ETA application. For this purpose, SAR techniques

This article has been accepted for publication in IEEE Antennas and Wireless Propagation Letters. This is the author's version which has not been fully edited and content may change prior to final publication. Citation information: DOI 10.1109/LAWP.2024.3378012

TABLE IV: Experimental parameters for the SAR measurement.

Centre frequency (GHz)	Bandwidth (GHz)	Number of frequencies	Synthetic aperture length (cm)	Target dimensions (cm)
24	4	3201	12	10×10

for high-resolution electromagnetic imaging are implemented to map the nearby environment. This is achieved by taking advantage of the natural movement of the body, so a resolution better than the one obtained with a single position, is reached [10].

Electromagnetic images are computed by means of a flexible sum-and-delay algorithm for monostatic acquisition [24]:

$$\hat{\rho}(\overrightarrow{r}') = \sum_{m=1}^{M}\sum_{n=1}^{N} S(m,n)\cdot e^{j2k_m\left|\overrightarrow{r}'-\overrightarrow{r}_n\right|}, \qquad (1)$$

in which $\rho(\overrightarrow{r}')$ stands for the reflectivity of the target, $\overrightarrow{r}'$ represents to the pixel where reflectivity will be calculated, S depicts the acquired data corresponding to the s_{11} parameter after subtracting the background and calibrating the phase shift, M indicates the number of frequencies and N refers to the acquisition points, k_m refers to the wavenumber at the m-th frequency and $\overrightarrow{r}_n$ appoints the n-th measured position.

Fig 6(a) depicted the pure monostatic set-up used to perform the measurements. A metallic plate of 10×10 cm has been used as a target. The movement of the antenna is recorded using a tracking camera. In particular, the Intel® RealSense™ Tracking Camera T265 [25] is used to register the measurement positions. The antenna and the camera have been placed in a 3D printed gadget, in order to move them together, as well as to fix them to the user's arm, as can be observed in Fig 6(b).

The antenna is moved by means of simple arm swings. The measurement point interval was cropped to 12 cm from the target as the tracking device accumulate positioning errors and only positions within a short period are consistent. The target was placed at 10 cm. The scattering parameter S is measured with a vector network analyzer (VNA), in order to emulate a stepped-frequency continuous-wave (SFCW) radar. Table IV summarizes the SAR configuration considerations set up to perform the measurement. It is necessary to clarify that the measurement has been conducted in an extended frequency band from 22 to 26 GHz, to obtain a good range resolution that allows to distinguish the target and its range position. The corresponding measurement dataset, can be found in [26].

Fig. 7 presents the electromagnetic image obtained with the AMC-antenna. Although there are artifacts due to the irregular sampling [27], the target is correctly detected at 10 cm from the radar, that has been highlighted in red color in the image, which agrees with its real position. The effects of irregular sampling can be mitigated by different technique such as the use of deep learning by means of transformers or generative adversarial networks as shown in [27], [28]. Besides, it can be observed that the target width (x-axis) matches the actual object size of 10 cm, as expected, since the resolution is

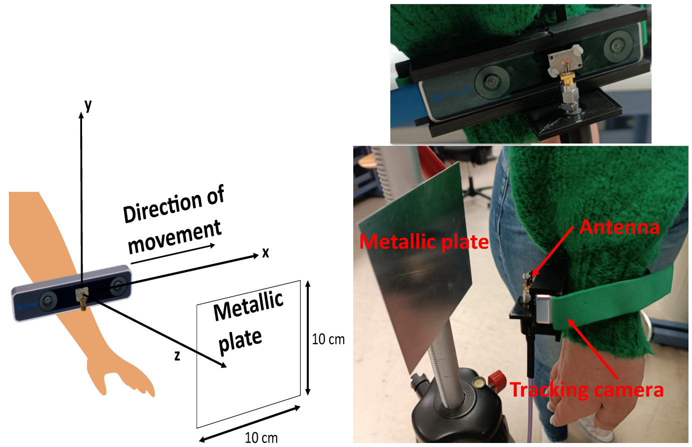

(a) (b)

Fig. 6: Measurement set-up. (a) Schematic, (b) Real laboratory set-up.

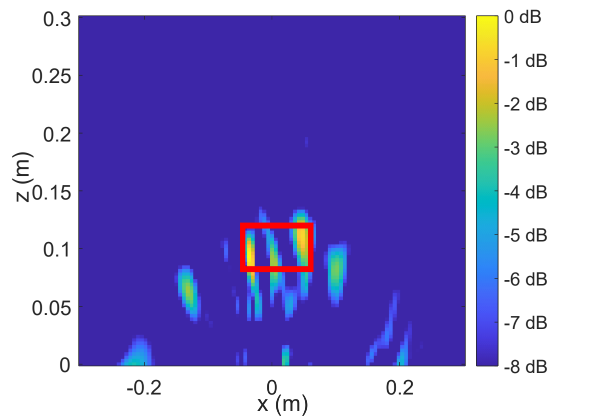

Fig. 7: Electromagnetic image obtained with the AMC-antenna.

only along the x-axis. Therefore, the antenna performance is suitable for the pursued application.

IV. Conclusions

A novel ultra-compact and lightweight AMC-backed twin arrow wearable antenna, suitable for ETA applications, has been achieved. The FTBR and radiation properties of the initial antenna have been improved by backing it with an AMC. Significant improvement has been obtained in the FTBR, which is key for the intended application, in order to avoid user radiation. In addition, the radiation parameters and the operation bandwidth of the antenna have been enhanced, without increasing its area.

The antenna performance has been validated for the case of close metallic targets. The experimental validation shows that the target can be correctly detecting providing the distance and an estimation of the profile, illustrating that the arm movement is exploited to improve the image with respect to one obtained with the antenna at a single position.

REFERENCES

[1] World Health Organization, January 2024. [Online] Available: https://www.who.int/news-room/fact-sheets/detail/blindness-and-visual-impairment.

[2] D. Abreu, J. Toledo, B. Codina, and A. Suárez, “Low-cost ultrasonic range improvements for an assistive device,” Sensors, vol. 21, no. 12, p. 4250, Jun. 2021, doi: 10.3390/s21124250.

[3] C. Gearhart, A. Herold, B. Self, C. Birdsong and L. Slivovsky, "Use of ultrasonic sensors in the development of an Electronic Travel Aid," 2009 IEEE Sensors Applications Symposium, New Orleans, LA, USA, 2009, pp. 275-280, doi: 10.1109/SAS.2009.4801815.

[4] A. S. Rao, J. Gubbi, M. Palaniswami and E. Wong, "A vision-based system to detect potholes and uneven surfaces for assisting blind people," 2016 IEEE International Conference on Communications (ICC), Kuala Lumpur, Malaysia, 2016, pp. 1-6, doi: 10.1109/ICC.2016.7510832.

[5] E. Cardillo and A. Caddemi, “Insight on electronic travel aids for visually impaired people: A review on the electromagnetic technology,” Electronics, vol. 8, no. 11, p. 1281, Nov. 2019, doi: 10.3390/electronics8111281.

[6] I. M. Skolnik, Introduction to RADAR Systems. New York, NY, USA: McGraw-Hill, 1980

[7] D. M. Sheen, D. L. McMakin, and T. E. Hall, “Three-dimensional millimeter-wave imaging for concealed weapon detection,” IEEE Trans. Microw. Theory Techn., vol. 49, no. 9, pp. 1581–1592, Sep. 2001, doi: 10.1109/22.942570

[8] S. Agarwal, B. Kumar and D. Singh, "Non-invasive concealed weapon detection and identification using V band millimeter wave imaging radar system," 2015 National Conference on Recent Advances in Electronics & Computer Engineering (RAECE), Roorkee, India, 2015, pp. 258-262, doi: 10.1109/RAECE.2015.7510202.

[9] M. T. Bevacqua, S. Di Meo, L. Crocco, T. Isernia and M. Pasian, "Millimeter-Waves Breast Cancer Imaging via Inverse Scattering Techniques," in IEEE Journal of Electromagnetics, RF and Microwaves in Medicine and Biology, vol. 5, no. 3, pp. 246-253, Sept. 2021, doi: 10.1109/JERM.2021.3052096.

[10] H. F. Álvarez, G. Álvarez-Narciandi, F. Las-Heras and J. Laviada, “System Based on Compact mmWave Radar and Natural Body Movement for Assisting Visually Impaired People,” in IEEE Access, vol. 9, pp. 125042-125051, 2021, doi: 10.1109/ACCESS.2021.3110582.

[11] A. F. Berdasco, J. Laviada, M. E. de Cos Gómez and F. Las-Heras, "Performance Evaluation of Millimeter-Wave Wearable Antennas for Electronic Travel Aid," in IEEE Transactions on Instrumentation and Measurement, vol. 72, pp. 1-10, 2023, Art no. 4507510, doi: 10.1109/TIM.2023.3320736.

[12] A. Flórez Berdasco, M.E. de Cos Gómez, H. Fernández Álvareza nd F. Las-Heras, “Millimeter wave array-HIS antenna for imaging applications,” in Appl. Phys. A 129, 397 (2023), doi: 10.1007/s00339-023-06676-0.

[13] M. Mantash, A.-C. Tarot, S. Collardey, and K. Mahdjoubi, “Design methodology for wearable antenna on artificial magnetic conductor using stretch conductive fabric,” Electron. Lett., vol. 52, no. 2, pp. 95–96, Jan. 2016.

[14] A. Alemaryeen and S. Noghanian, "On-Body Low-Profile Textile Antenna With Artificial Magnetic Conductor," in IEEE Transactions on Antennas and Propagation, vol. 67, no. 6, pp. 3649-3656, June 2019, doi: 10.1109/TAP.2019.2902632.

[15] Ayd R. Saad, A., Hassan, W.M. & Ibrahim, A.A. A monopole antenna with cotton fabric material for wearable applications. Sci Rep 13, 7315 (2023). doi: 10.1038/s41598-023-34394-3

[16] K Srilatha et al 2021 J. Phys.: Conf. Ser. 1804 012189

[17] Saha, P. & Mitra, D. & Parui, S.K.. (2021). Control of Gain and SAR for Wearable Antenna Using AMC Structure. Radioengineering, vol. 30, pp. 81-88. doi: 10.13164/re.2021.0081.

[18] Fan Yang and Y. Rahmat-Samii, "Reflection phase characterizations of the EBG ground plane for low profile wire antenna applications," in IEEE Transactions on Antennas and Propagation, vol. 51, no. 10, pp. 2691-2703, Oct. 2003, doi: 10.1109/TAP.2003.817559.

[19] J. Bito, V. Palazzi, J. Hester, R. Bahr, F. Alimenti, P. Mezzanotte, L. Roselli, M. M. Tentzeris, “Millimeter-wave ink-jet printed RF energy harvester for next generation flexible electronics,” 2017 IEEE Wireless Power Transfer Conference (WPTC), Taipei, Taiwan, 10–12 May 2017; pp. 1–4.

[20] P. Mezzanotte, C. Mariotti, M. Virili, M. Poggiani, G. Orecchini, F. Alimenti and L. Roselli, “24-GHz Patch antenna array on cellulose-based materials for green wireless internet applications,” IET Science, Measurement & Technology,vol. 8 pp. 342-349, 2014

[21] N. Kathuria, B.-C. Seet, “24 GHz Flexible Antenna for Doppler Radar-Based Human Vital Signs Monitoring,” Sensors 2021, 21, 3737.

[22] Park S, Kim S, Kim DK, Choi J, Jung K-Y. “Numerical Study on the Feasibility of a 24 GHz ISM-Band Doppler Radar Antenna for Near-Field Sensing of Human Respiration in Electromagnetic Aspects,” Applied Sciences. 2020; 10(18):6159, doi: 10.3390/app10186159.

[23] F. A. Ghaffar, M. U. Khalid, K. N. Salama and A. Shamim, “24-GHz LTCC Fractal Antenna Array SoP With Integrated Fresnel Lens,” IEEE Antennas and Wireless Propagation Letters, vol. 10, pp. 705-708, 2011.

[24] M. Soumekh, Synthetic Aperture Radar Signal Processing, New York, NY, USA: Wiley, vol. 7, 1999.

[25] Intel® RealSense™ Tracking Camera T265, January 2024. [Online] Available: https://www.intelrealsense.com/visual-inertial-tracking-case-study/.

[26] Alicia Florez Berdasco, María Elena de Cos Gómez , Jaime Laviada, Fernando Las-Heras, February 1, 2024, "Experimental SAR measurements for electronic travel aid purposes", IEEE Dataport, doi: https://dx.doi.org/10.21227/dcdt-1e95.

[27] J. W. Smith, Y. Alimam, G. Vedula and M. Torlak, "A Vision Transformer Approach for Efficient Near-Field SAR Super-Resolution under Array Perturbation," 2022 IEEE Texas Symposium on Wireless and Microwave Circuits and Systems (WMCS), Waco, TX, USA, 2022, pp. 1-6, doi: 10.1109/WMCS55582.2022.9866326

[28] J. Laviada, G. Álvarez-Narciandi and F. Las-Heras, "Artifact Mitigation for High-Resolution Near-Field SAR Images by Means of Conditional Generative Adversarial Networks," in IEEE Transactions on Instrumentation and Measurement, vol. 71, pp. 1-11, 2022, Art no. 8006011, doi: 10.1109/TIM.2022.3200107